Hybridization of electron, light-hole, and heavy-hole states in InAs/GaSb quantum wells

A. Zakharova
Physics Division, National Center for Theoretical Sciences, Hsinchu, Taiwan, Republic of China, and Institute of Physics and Technology, RAS, Nakhimovskii Avenue 34, Moscow 117218, Russia

S. T. Yen
Department of Electronics Engineering, National Chiao Tung University, Hsinchu, Taiwan, Republic of China

K. A. Chao
Department of Physics, Lund University, Sölvegutun 14A, S 233 62 Lund, Sweden
(Received 22 June 2001; published 29 November 2001)

We have investigated the hybridization of the electron states, the light-hole states and the heavy-hole states in InAs/GaSb broken-gap quantum wells. This effect is profound when the InAs layer and the GaSb layer are sufficiently thick such that the electron level lies below the heavy-hole level and the light-hole level at zone center. To calculate the dispersions and the wave functions in these structures we have applied the scattering matrix algorithm to the eight-band $\mathbf{k}\cdot\mathbf{p}$ model. We have found a hybridization gap as large as 20 meV resulting from the anticrossing of the electron and the light-hole dispersion curves. A multiple anticrossing of the electron states, the light-hole states and the heavy-hole states may occur when the heavy hole level lies in the hybridization gap produced by the electron states and the light-hole states. This unusual hybridization of the three subbands, which behaves differently for the ''spin-up'' and the ''spin-down'' states, has been investigated in details around the anticrossing point. While the electronlike and light holelike states mix strongly, the heavy holelike state may remain unperturbed.

DOI: 10.1103/PhysRevB.64.235332 PACS number(s): 73.40.Gk, 73.40.Kp

I. INTRODUCTION

In broken-gap heterostructures such as InAs/GaSb, the conduction band of InAs overlaps with the valence band of GaSb. They exhibit unusual physical properties which are of interest to both fundamental research and device applications. The InAs/GaSb resonant tunneling structures,[1–4] the InAs/GaSb/AlSb infrared detectors and laser diode structures,[5–7] the AlSb/InAs/GaSb/AlSb quantum wells,[8–11] and the InAs/GaSb superlattices[12,13] have been fabricated and investigated. In these structures the conduction band states in InAs couple strongly to the valence band states in GaSb, resulting in a significant interband tunneling transport between the electronlike levels and the holelike levels when they are separated by a weak barrier.[1–4] The electron-hole coupling in the quantum well structures and the superlattices gives rise to a large optical absorption coefficient and an efficient stimulated emission at room temperature.[5–7] The coupling-induced charge transfer between the InAs layer and the GaSb layer manifests itself in a switch between the hole-dominating transport and the electron-dominating transport. By varying the InAs layer thickness and the GaSb layer thickness in a quantum well, at zone center (the in-plane wave vector $\mathbf{k}_{\|}=0$) the electronlike level can be pushed below the heavy-hole level. Hence, an anticrossing phenomenon may occur at a finite value of $\mathbf{k}_{\|}$. The so-produced small hybridization gap (<10 meV) in the in-plane dispersion has been observed recently.[10–13]

The electronic states of broken-gap heterostructures have been studied with the $\mathbf{k}\cdot\mathbf{p}$ method,[13–19] the tight-binding method,[20,21] the pseudopotential plane wave approach,[22,23] and the effective bond orbital model.[24,25] Band structure calculations have suggested interesting features in the in-plane dispersions of InAs/GaSb superlattices,[13–15,22,23] as well as of InAs/GaSb quantum well structures.[16,17,19,24,25] The opening of a hybridization gap as the InAs and the GaSb layer thicknesses change was already mentioned above. Due to the spin-orbit interaction which may be significant in asymmetrical structures, the in-plane dispersions become spin dependent.[25] Hence, the magnitudes of the hybridization gaps depend also on the spin orientation.

In this paper we will investigate the features of hybridized dispersions and the associated wave functions in InAs/GaSb quantum wells. We will use an eight-band $\mathbf{k}\cdot\mathbf{p}$ model to construct the bulk states in all layers, and then match the wave functions at interfaces with the boundary conditions of Burt's envelope function theory.[26,27] We will generalize the scattering matrix algorithm, which was proposed in Ref. 28 for calculating the transmission coefficients, to calculate the energy levels. This algorithm does not invoke the inversion of nearly singular matrices and so avoids the problem of numerical instability when the quantum well thickness increases. Recently, thick InAs/GaSb quantum wells have been investigated experimentally.[12]

In Sec. II we present the theoretical model for the investigation of electronic band structures using the eight-band $\mathbf{k}\cdot\mathbf{p}$ method. The scattering matrix algorithm is then described in Sec. III, and the calculated dispersions and wave functions are discussed thoroughly in Sec. IV. Due to the strong coupling between electrons and light holes, the resulting energy gap can be as large as 20 meV. We have analyzed the unusual features of wave functions when the electron, the heavy-hole, and the light-hole dispersion curves anticross simultaneously. It is interesting to see the complicated behav-

 ©2001 The American Physical Society

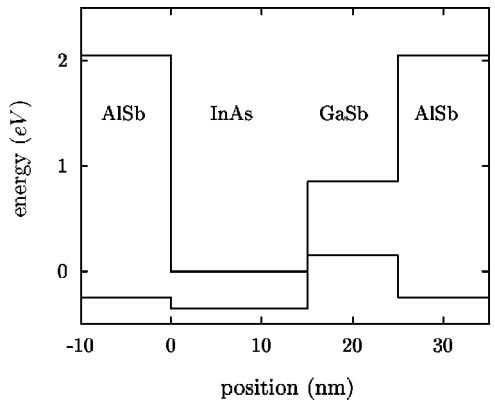

FIG. 1. Conduction and valence band diagrams of the AlSb/InAs/GaSb/AlSb broken-gap quantum well structure.

ior of wave functions when a heavy-hole-like energy level lies within the gap produced by the hybridization between the electronlike and the light-hole-like states. A conclusion is reached in the final Sec. V.

II. MODEL DESCRIPTION

We consider an InAs/GaSb broken-gap quantum well embedded in two wide gap AlSb layers, as shown in Fig. 1. The energy band structure calculation is based on the eight-band $\mathbf{k}\cdot\mathbf{p}$ model for the Γ point of zinc blende crystals, including the two lowest conduction bands and the six highest valence bands. The growth direction $\langle 010\rangle$ of our sample is defined as the *y* axis. In order to obtain concrete numerical results for analyzing the physical properties, we will derive the in-plane dispersion relation along the $\langle 100\rangle$ direction, which we will take as the *x* axis. Then, in terms of the basis functions

$$u_1=|s_{1/2,1/2}\rangle=i|S\uparrow\rangle, \tag{1a}$$

$$u_2=|p_{3/2,3/2}\rangle=\frac{-i}{\sqrt{2}}|(X+iY)\uparrow\rangle, \tag{1b}$$

$$u_3=|p_{3/2,-1/2}\rangle=i\sqrt{\frac{1}{6}}|(X-iY)\uparrow\rangle+i\sqrt{\frac{2}{3}}|Z\downarrow\rangle, \tag{1c}$$

$$u_4=|p_{1/2,-1/2}\rangle=i\sqrt{\frac{1}{3}}|(X-iY)\uparrow\rangle-i\sqrt{\frac{1}{3}}|Z\downarrow\rangle, \tag{1d}$$

$$u_5=|s_{1/2,-1/2}\rangle=i|S\downarrow\rangle, \tag{1e}$$

$$u_6=|p_{3/2,-3/2}\rangle=\frac{i}{\sqrt{2}}|(X-iY)\downarrow\rangle, \tag{1f}$$

$$u_7=|p_{3/2,1/2}\rangle=-i\sqrt{\frac{1}{6}}|(X+iY)\downarrow\rangle+i\sqrt{\frac{2}{3}}|Z\uparrow\rangle, \tag{1g}$$

$$u_8=|p_{1/2,1/2}\rangle=-i\sqrt{\frac{1}{3}}|(X+iY)\downarrow\rangle-i\sqrt{\frac{1}{3}}|Z\uparrow\rangle, \tag{1h}$$

the 8×8 Hamiltonian matrix can be written in the block diagonal form[26,27]

$$\hat{H}=\begin{pmatrix}\hat{H}_+ & 0\\ 0 & \hat{H}_-\end{pmatrix}. \tag{2}$$

The 4×4 blocks $\hat{H}_\pm$

$$\hat{H}_\pm=\begin{pmatrix}\hat{H}_{cc} & P\hat{k}_\pm & P\hat{k}_\mp/\sqrt{3} & \sqrt{2}P\hat{k}_\mp/\sqrt{3}\\ \hat{k}_\mp P & E_v+\hat{F}_\pm & \hat{R}_\mp & \sqrt{2}\hat{R}_\mp\\ \hat{k}_\pm/\sqrt{3}P & \hat{R}_\pm & E_v+\hat{G}_\mp & \hat{D}_\mp\\ \sqrt{2}\hat{k}_\pm/\sqrt{3}P & \sqrt{2}\hat{R}_\pm & \hat{D}_\mp & E_v+\hat{E}_\mp-\Delta\end{pmatrix}, \tag{3}$$

contain the operators

$$\hat{k}_\pm=\mp i(\hat{k}_x\pm i\hat{k}_y)/\sqrt{2}, \tag{4}$$

$$\hat{H}_{cc}=E_c+\hat{\mathbf{k}}A_c\hat{\mathbf{k}}, \tag{5}$$

$$\hat{G}_\pm=\frac{\hbar^2}{2m}[\hat{k}_+(\gamma_2-\gamma_1)\hat{k}_-+\hat{k}_-(\gamma_2-\gamma_1)\hat{k}_+]$$
$$\mp\frac{1}{6}[\hat{k}_+(N_+-N_-)\hat{k}_--\hat{k}_-(N_+-N_-)\hat{k}_+], \tag{6}$$

$$\hat{F}_\pm=-\frac{\hbar^2}{2m}[\hat{k}_+(\gamma_2+\gamma_1)\hat{k}_-+\hat{k}_-(\gamma_2+\gamma_1)\hat{k}_+]$$
$$\mp\frac{1}{2}[\hat{k}_+(N_+-N_-)\hat{k}_--\hat{k}_-(N_+-N_-)\hat{k}_+], \tag{7}$$

$$\hat{E}_\pm=-\frac{\hbar^2}{2m}[\hat{k}_+\gamma_1\hat{k}_-+\hat{k}_-\gamma_1\hat{k}_+]$$
$$\mp\frac{1}{3}[\hat{k}_+(N_+-N_-)\hat{k}_--\hat{k}_-(N_+-N_-)\hat{k}_+], \tag{8}$$

$$\hat{R}_\pm=-\frac{\hbar^2\sqrt{3}}{2m}[\hat{k}_+\gamma_2\hat{k}_++\hat{k}_-\gamma_2\hat{k}_-]$$
$$\mp\frac{1}{2\sqrt{3}}(\hat{k}_-N\hat{k}_--\hat{k}_+N\hat{k}_+), \tag{9}$$

and

$$\hat{D}_\pm=-\frac{\hbar^2}{2m}\sqrt{2}[\hat{k}_+\gamma_2\hat{k}_-+\hat{k}_-\gamma_2\hat{k}_+]$$
$$\mp\frac{1}{3\sqrt{2}}[\hat{k}_+(N_+-N_-)\hat{k}_--\hat{k}_-(N_+-N_-)\hat{k}_+]. \tag{10}$$

In the above equations, P is the interband momentum matrix element, E_c the conduction band edge, E_v the valence band edge, and Δ the split-off energy. γ_1, γ_2, and γ_3 are the

modified Luttinger parameters, with m as the free electron mass. The effect of remote bands on the electron effective mass is contained in A_c. All these parameters depend on material, and thus are functions of y. Therefore, their orders with the momentum operators are important. N_+ and N_- can be expressed in terms of the modified Luttinger parameters as

$$N_- = -(\hbar^2/2m)(\gamma_1 - 2\gamma_2 + 1), \tag{11}$$

$$N_+ = -(\hbar^2/2m)(6\gamma_3 - \gamma_1 + 2\gamma_2 - 1), \tag{12}$$

and $N = N_+ + N_-$. In writing the block diagonal form of the Halmiltonian in Eq. (2), we have neglected terms containing Kane's asymmetry parameter B and set k_z to be zero. The linear-in-**k** terms of the spin-orbit interaction have also been dropped since their effect is very small compared to that of the k-independent spin-orbit interaction for the range of in-plane wave vectors that we are interested in. The envelope functions ψ_i and the corresponding eigenenergies E are then obtained by solving the equations

$$\sum_{j=1}^{8} \hat{H}_{ij}\psi_j = E\psi_i, \quad i = 1,2,\ldots,8. \tag{13}$$

It has been shown[27] that if A_c is finite, spurious solutions with large real wave vectors appear in the band gaps of zinc blende crystals. To eliminate these nonphysical solutions, one sets $A_c = 0$ and uses the remaining empirical parameters to include the effect of remote bands on the electron effective mass, as described in Ref. 27. Since the Hamiltonian has a block-diagonal form, we can solve separately the equations for the ''spin-up'' block $\hat{H}_+$ and the ''spin-down'' block $\hat{H}_-$. In fact, we need to solve the equations for the ''spin-up'' states only, because due to the time reversal symmetry, the dispersions for the ''spin-down'' states can be obtained from those of the ''spin-up'' states by changing the sign of the in-plane wave vector.

From the first ($i = 1$) of the eight equations in Eq. (13), the conduction band envelope function of the ''spin-up'' states can be expressed in terms of the valence band envelope functions as

$$\psi_1 = \frac{P}{E - E_c}(\hat{k}_+\psi_2 + \hat{k}_-\psi_3/\sqrt{3} + \sqrt{2}\hat{k}_-\psi_4/\sqrt{3}). \tag{14}$$

The conduction band envelope function for the ''spin-down'' states, ψ_5, can be expressed in a similar way. Consequently, the problem of the 4×4 block matrix $\hat{H}_+$ reduces to that of the 3×3 block matrix Hamiltonian

$$\hat{H}'_+ = \begin{pmatrix} E_v + \hat{F}'_+ & \hat{R}'_- & \sqrt{2}\hat{R}'_- \\ \hat{R}'_+ & E_v + \hat{G}'_- & \hat{D}'_- \\ \sqrt{2}\hat{R}'_+ & \hat{D}'_- & E_v + \hat{E}'_- - \Delta \end{pmatrix}, \tag{15}$$

where the elements $\hat{G}'_-$, $\hat{F}'_+$, $\hat{E}'_-$, $\hat{R}'_\pm$, and $\hat{D}'_-$ are obtained from the corresponding elements given by Eqs. (6)–(10) by replacing N, N_+, γ_1, γ_2, and γ_3 with

$$N' = N + \frac{P^2}{E - E_c}, \tag{16}$$

$$N'_+ = N_+ + \frac{P^2}{E - E_c}, \tag{17}$$

$$\gamma'_1 = \gamma_1 - \frac{E_p}{3(E - E_c)}, \tag{18}$$

$$\gamma'_2 = \gamma_2 - \frac{E_p}{6(E - E_c)}, \tag{19}$$

$$\gamma'_3 = \gamma_3 - \frac{E_p}{6(E - E_c)}. \tag{20}$$

Here $E_p = 2mP^2/\hbar^2$. The equation for the valence band envelope functions of the ''spin-up'' states then becomes

$$\hat{H}'\mathbf{\Psi} = E\mathbf{\Psi}, \quad \mathbf{\Psi} = [\psi_2\ \psi_3\ \psi_4]^T. \tag{21}$$

III. SCATTERING MATRIX ALGORITHM

In the conventional transfer matrix method, the coefficients of the forward and the backward waves in one layer are determined by those of the front layer and proper boundary conditions. This method may, however, give rise to instability in numerical results as a rapid growing wave and a rapid decaying wave are both present in a thick layer. In this case, the decaying wave is overwhelmed and neglected compared to the growing wave at one of the boundaries of this layer. Consequently, it is impossible to determine definitely the coefficient of the neglected decaying wave. In the present work, we use the scattering matrix algorithm in calculation of band structures to avoid the problem with the transfer matrix technique. In this method, the coefficients of the outgoing waves are obtained definitely from those of the incoming waves through the scattering matrix.

The envelope functions of the entire heterostructure are constructed as linear combinations of the bulk eigenstates in each layer. For the nth layer the bulk eigenstates can be expressed in forms of plane wave $\mathbf{e}^{(n)}\exp[ik_x x + ik_y^{(n)} y]$, where $\mathbf{e}^{(n)}$ is a 3×1 column vector: $\mathbf{e}^{(n)} = [e_2^{(n)}\ e_3^{(n)}\ e_4^{(n)}]^T$. Substituting the bulk eigenstates into Eq. (21), we arrive at an equation for the dispersions and the eigenvectors of the nth layer

$$(B_2^{(n)}k_y^{(n)2} + B_1^{(n)}ik_y^{(n)} + B_0^{(n)})\mathbf{e}^{(n)} = 0. \tag{22}$$

The matrices $B_2^{(n)}$, $B_1^{(n)}$, $B_0^{(n)}$ are given by

$$B_2^{(n)} = \begin{pmatrix} -(\gamma'_2 + \gamma'_1) & -\sqrt{3}\gamma'_2 & -\sqrt{6}\gamma'_2 \\ -\sqrt{3}\gamma'_2 & \gamma'_2 - \gamma'_1 & -\sqrt{2}\gamma'_2 \\ -\sqrt{6}\gamma'_2 & -\sqrt{2}\gamma'_2 & -\gamma'_1 \end{pmatrix}, \tag{23}$$

$$B_1^{(n)} = k_x \begin{pmatrix} 0 & -2\sqrt{3}\gamma_3' & -2\sqrt{6}\gamma_3' \\ 2\sqrt{3}\gamma_3' & 0 & 0 \\ 2\sqrt{6}\gamma_3' & 0 & 0 \end{pmatrix}, \quad (24)$$

$$B_0^{(n)} = k_x^2 \begin{pmatrix} -(\gamma_2'+\gamma_1') & \sqrt{3}\gamma_2' & \sqrt{6}\gamma_2' \\ \sqrt{3}\gamma_2' & (\gamma_2'-\gamma_1') & -\sqrt{2}\gamma_2' \\ \sqrt{6}\gamma_2' & -\sqrt{2}\gamma_2' & -\gamma_1' \end{pmatrix} - \begin{pmatrix} \epsilon & 0 & 0 \\ 0 & \epsilon & 0 \\ 0 & 0 & \epsilon+\delta \end{pmatrix}, \quad (25)$$

where $\epsilon = 2m(E-E_v)/\hbar^2$ and $\delta = 2m\Delta/\hbar^2$.

The nontrivial solutions of Eq. (22) satisfy a third order polynomial equation in $k_y^{(n)2}$, in which the coefficients depend on E and k_x. For a given E and k_x, there are six complex solutions $\pm k_{y,i}^{(n)}$ with $i=1, 2, 3$, for the six corresponding eigenvectors $\mathbf{e}_{\pm i}^{(n)}$. Then, the envelope functions of the entire heterostructure in the nth layer can be written as

$$\mathbf{\Psi} = \exp(ik_x x) \sum_{j=1,2,3} [a_j^{(n)} \exp[ik_{y,j}^{(n)}(y-y_{n-1})] \times \mathbf{e}_{+j}^{(n)} + b_j^{(n)} \exp[-ik_{y,j}^{(n)}(y-y_n)]\, \mathbf{e}_{-j}^{(n)}]]. \quad (26)$$

In the above equation, y_{n-1} and y_n are the y coordinates which define the left and right boundaries of the nth layer. The coefficients $a_j^{(n)}$ and $b_j^{(n)}$ are for, respectively, the forward and the backward waves in the nth layer. They are determined by the boundary conditions, which are derived by integrating Eq. (21) across an interface. We define a matrix $\hat{H}_B$ as

$$\hat{H}_B(k_x, \hat{k}_y) = \begin{pmatrix} \hat{F}^B & \hat{R}_-^B & \sqrt{2}\hat{R}_-^B \\ \hat{R}_+^B & \hat{G}^B & \hat{D}^B \\ \sqrt{2}\hat{R}_+^B & \hat{D}^B & \hat{E}^B \end{pmatrix}, \quad (27)$$

where

$$\hat{F}^B = \frac{\hbar^2}{2m} i(\gamma_1'+\gamma_2')\hat{k}_y - \frac{1}{2}(N_+'-N_-)k_x, \quad (28)$$

$$\hat{R}_\pm^B = \frac{\hbar^2}{2m} i\sqrt{3}\gamma_2'\hat{k}_y \mp \frac{1}{2\sqrt{3}} N' k_x, \quad (29)$$

$$\hat{G}^B = -\frac{\hbar^2}{2m} i(\gamma_2'-\gamma_1')\hat{k}_y + \frac{1}{6}(N_+'-N_-)k_x, \quad (30)$$

$$\hat{D}^B = \frac{\hbar^2}{2m} i\sqrt{2}\gamma_2'\hat{k}_y + \frac{1}{3\sqrt{2}}(N_+'-N_-)k_x, \quad (31)$$

$$\hat{E}^B = \frac{\hbar^2}{2m} i\gamma_1'\hat{k}_y + \frac{1}{3}(N_+'-N_-)k_x. \quad (32)$$

The boundary conditions then imply that the vector functions $\mathbf{\Psi}$ and $\hat{H}_B\mathbf{\Psi}$ are continuous at each interface.

Under these boundary conditions, the coefficients for two neighbor layers can be connected by a transfer matrix

$$M^{(n+1)} = \begin{pmatrix} D^{(n)-1} & 0 \\ 0 & I \end{pmatrix} \overline{M}^{(n+1)} \begin{pmatrix} I & 0 \\ 0 & D^{(n+1)} \end{pmatrix} \quad (33)$$

as

$$\begin{pmatrix} \mathbf{a}^{(n)} \\ \mathbf{b}^{(n)} \end{pmatrix} = M^{(n+1)} \begin{pmatrix} \mathbf{a}^{(n+1)} \\ \mathbf{b}^{(n+1)} \end{pmatrix}, \quad (34)$$

where I is the 3×3 identity matrix, and $D^{(n)}$ is a 3×3 diagonal matrix with the elements

$$D_{ij}^{(n)} = \delta_{ij} \exp[ik_{y,j}^{(n)}(y_n - y_{n-1})]. \quad (35)$$

Since matrix $D^{(n)}$ is diagonal, its inversion can be obtained by inverting each matrix element. $\overline{M}^{(n+1)}$ is a nonsingular invertible matrix which can be expressed as

$$\overline{M}^{(n+1)} = \begin{pmatrix} \mathbf{e}_+^{(n)} & \mathbf{e}_-^{(n)} \\ \mathbf{f}_+^{(n)} & \mathbf{f}_-^{(n)} \end{pmatrix}^{-1} \begin{pmatrix} \mathbf{e}_+^{(n+1)} & \mathbf{e}_-^{(n+1)} \\ \mathbf{f}_+^{(n+1)} & \mathbf{f}_-^{(n+1)} \end{pmatrix}, \quad (36)$$

where $\mathbf{e}_\pm^{(n)} = (\mathbf{e}_{\pm1}^{(n)}\ \mathbf{e}_{\pm2}^{(n)}\ \mathbf{e}_{\pm3}^{(n)})$ and $\mathbf{f}_\pm^{(n)} = (\mathbf{f}_{\pm1}^{(n)}\ \mathbf{f}_{\pm2}^{(n)}\ \mathbf{f}_{\pm3}^{(n)})$, $\mathbf{f}_{\pm j}^{(n)} = \hat{H}_B \mathbf{e}_{\pm j}^{(n)}$, where in operator $\hat{H}_B$, $\hat{k}_y$ is replaced by $\pm k_{y,j}^{(n)}$.

The coefficients $\mathbf{a}^{(n)}$ and $\mathbf{b}^{(m)}$ of the outgoing waves and the coefficients $\mathbf{a}^{(m)}$ and $\mathbf{b}^{(n)}$ of the incoming waves are connected by a scattering matrix $S(m,n)$ as

$$\begin{pmatrix} \mathbf{a}^{(n)} \\ \mathbf{b}^{(m)} \end{pmatrix} = S(m,n) \begin{pmatrix} \mathbf{a}^{(m)} \\ \mathbf{b}^{(n)} \end{pmatrix}. \quad (37)$$

Using Eqs. (34) and (37), we can derive the following recursive formula for submatrices $S_{ij}(m,n)$ of the scattering matrix[28]

$$S_{11}(1,n+1) = [I - M_{11}^{(n+1)-1} S_{12}(1,n) M_{21}^{(n+1)}]^{-1} \times M_{11}^{(n+1)-1} S_{11}(1,n), \quad (38a)$$

$$S_{12}(1,n+1) = [I - M_{11}^{(n+1)-1} S_{12}(1,n) M_{21}^{(N+1)}]^{-1} \times M_{11}^{(n+1)-1} [S_{12}(1,n) M_{22}^{(n+1)} - M_{12}^{(n+1)}], \quad (38b)$$

$$S_{21}(1,n+1) = S_{22}(1,n) M_{21}^{(n+1)} S_{11}(1,n+1) + S_{21}(1,n), \quad (38c)$$

$$S_{22}(1,n+1) = S_{22}(1,n) M_{21}^{(n+1)} S_{12}(1,n+1) + S_{22}(1,n) M_{22}^{(n+1)}. \quad (38d)$$

The submatrices of $M^{(n+1)}$ are obtained from Eq. (33) as

$$M_{11}^{(n+1)-1} = \overline{M}_{11}^{(n+1)-1} D^{(n)}, \quad (39a)$$

$$M_{12}^{(n+1)} = D^{(n)-1} \overline{M}_{12}^{(n+1)} D^{(n+1)}, \quad (39b)$$

$$M_{21}^{(n+1)} = \overline{M}_{21}^{(n+1)}, \quad (39c)$$

$$M_{22}^{(n+1)} = \overline{M}_{22}^{(n+1)} D^{(n+1)}. \tag{39d}$$

Setting $S(1,1)$ to be the identity matrix, from the recursive relations (38) we can construct all the scattering matrices $S(1,n)$ for $n=2,3,\ldots,N$. Similarly, setting $S(m,m)=I$, all matrices $S(m,n)$ with $n=m+1,m+2,\ldots,N$, can be found.

Then using Eq. (37) we can derive the following relations:

$$\mathbf{a}^{(m)} = S_{11}(1,m)\mathbf{a}^{(1)} + S_{12}(1,m)\mathbf{b}^{(m)}, \tag{40a}$$

$$\mathbf{b}^{(1)} = S_{21}(1,m)\mathbf{a}^{(1)} + S_{22}(1,m)\mathbf{b}^{(m)}, \tag{40b}$$

$$\mathbf{a}^{(N)} = S_{11}(m,N)\mathbf{a}^{(m)} + S_{12}(m,N)\mathbf{b}^{(N)}, \tag{40c}$$

$$\mathbf{b}^{(m)} = S_{21}(m,N)\mathbf{a}^{(m)} + S_{22}(m,N)\mathbf{b}^{(N)}, \tag{40d}$$

where $\mathbf{a}^{(1)}$ and $\mathbf{b}^{(1)}$ are the coefficients for the left barrier layer, while $\mathbf{a}^{(N)}$ and $\mathbf{b}^{(N)}$ are for the right barrier layer. We set the coefficients of incoming waves $\mathbf{a}^{(1)}$ and $\mathbf{b}^{(N)}$ to be zero to determine the energy levels of the states confined to the quantum well. Substituting Eq. (40a) into Eq. (40d), we have the equation

$$[I - S_{21}(m,N)S_{12}(1,m)]\mathbf{b}^{(m)} = 0, \tag{41}$$

from which the energy levels and the corresponding coefficients $\mathbf{b}^{(m)}$ are derived. Knowing $\mathbf{b}^{(m)}$, the coefficients $\mathbf{a}^{(m)}$, $\mathbf{b}^{(1)}$, and $\mathbf{a}^{(N)}$ are readily obtained from Eqs. (40a), (40b), and (40c), respectively.

IV. RESULTS AND DISCUSSION

For our numerical calculation on the InAs/GaSb broken-gap quantum well as shown in Fig. 1, the material parameters such as values of the energy gap, the split-off energy, the interband momentum matrix elements, and the Luttinger parameters are taken from Ref. 25. In contrast to the case studied in Ref. 25, we will consider thicker quantum wells such that at $k_\parallel = 0$ the first electron level lies below the first light hole level. Several heavy hole levels are then also above the first electron level. Then multiple electron-hole anticrossings can produce multiple minigaps. Such effect in long-period superlattices has been discussed recently.[23] Because the spin-orbit interaction breaks the double spin degeneracy in an asymmetric quantum well, we will see that for a finite value of $k_\parallel$, the dispersion curves and the spatial probability densities are different for the ''spin-up'' states and the ''spin-down'' states. This phenomenon was also detected in Ref. 25.

For a given InAs layer thickness and a GaSb layer thickness in the AlSb/InAs/GaSb/AlSb broken-gap quantum well structure, we investigate the band structure as well as the spatial distribution of the probability density for the zone center states and for the states in the vicinity of anticrossing. The results for the structure with a 15 nm InAs layer and a 10 nm GaSb layer are shown in Figs. 2, 3, and 4. Choosing the InAs conduction band edge as the zero reference energy, the dispersions are plotted in Fig. 2(a) for the ''spin-up'' states, and Fig. 2(b) for the ''spin-down'' states. There are six subbands of interest, labeled as $1hh$, $2hh$, $3hh$, for heavy-hole states, $1lh$ for light-hole states, and $1e$, $2e$ for electrons. The assignment of carrier type to various subbands follows the associated wave function properties at $k_\parallel = 0$. As is well known, such symmetry can no longer be defined for a finite value of $k_\parallel$. The in-plane wave vector is measured in units nm^{-1}, and for our system the wave vectors at the zone boundaries are about $\pm 10\ \mathrm{nm}^{-1}$. At the zone center there is only a weak coupling between the conduction band states and the states in light-hole bands. With increasing $k_\parallel$ the coupling strength between the electrons and the light holes is much enhanced, resulting a large hybridization gap of about

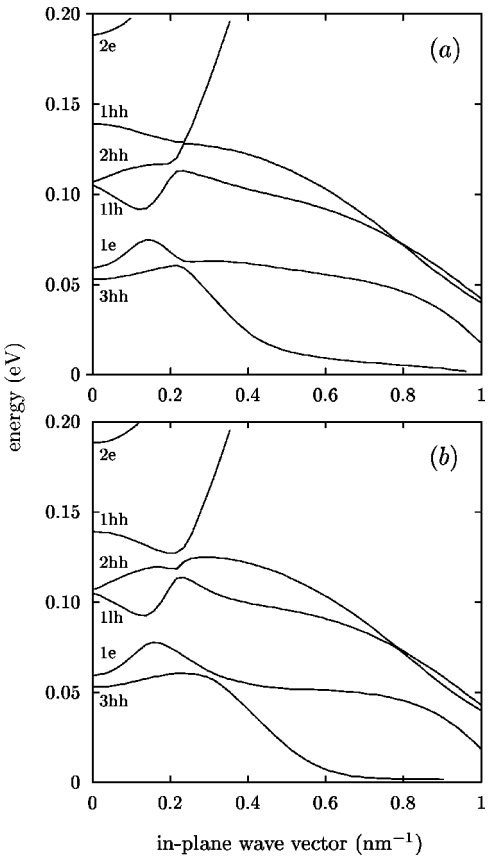

FIG. 2. Subband dispersions for the quantum well structure with a 15 nm InAs layer and a 10 nm GaSb layer.

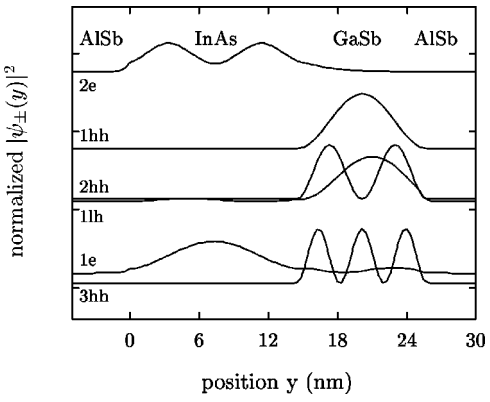

FIG. 3. Normalized probability density $|\psi_\pm(y)|^2$ for the zone center states in a quantum well with a 15 nm InAs layer and a 10 nm GaSb layer.

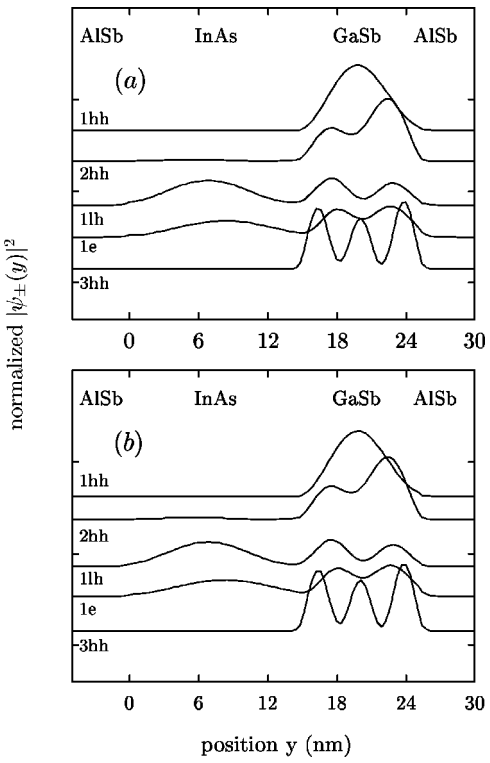

FIG. 4. Normalized probability density $|\psi_+(y)|^2$ of the "spin-up" states [panel (a)] and $|\psi_-(y)|^2$ of the "spin-down" states [panel (b)] at $k_\parallel = 0.14\ \mathrm{nm}^{-1}$ in a quantum well with a 15 nm InAs layer and a 10 nm GaSb layer.

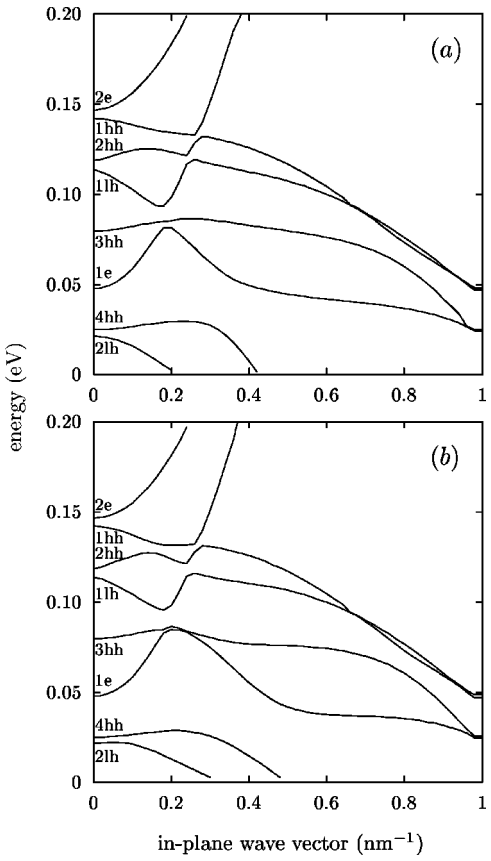

FIG. 5. Subband dispersions for the quantum well structure with an 18 nm InAs layer and a 12 nm GaSb layer.

20 meV around $k_\parallel = 0.14\ \mathrm{nm}^{-1}$. At the same time, the coupling between electron states and heavy-hole states develops, causing the complicated multiple anticrossings. This can be seen around $k_\parallel = 0.2\ \mathrm{nm}^{-1}$ where the three $1hh$, $2hh$, and $1lh$ subbands are separated by two hybridization gaps. With further increase of $k_\parallel$, the anticrossing between the $1e$ subband and the $3hh$ subband occurs. The position and the magnitude of each hybridization gap are spin dependent.

The hybridization phenomenon can be demonstrated more clearly with the probability density $|\psi_+(y)|^2 = \Sigma_{i=1}^{4}|\psi_i(y)|^2$ for a "spin-up" state, and $|\psi_-(y)|^2 = \Sigma_{i=5}^{8}|\psi_i(y)|^2$ for a "spin-down" state. Because of the spin-degeneracy at the zone center $|\psi_+(y)|^2 = |\psi_-(y)|^2$, and the results are plotted in Fig. 3. Each probability density is normalized to unity, and the curves are displaced and ordered according to their corresponding energies at the zone center. The flat parts at both sides of each curve mark the zero reference $|\psi_+(y)|^2 = 0$ or $|\psi_-(y)|^2 = 0$. We see clearly that only the electron states and the light-hole states are weakly coupled. As a result, the heavy-holes are confined in the GaSb layer.

The difference between $|\psi_+(y)|^2$ and $|\psi_-(y)|^2$ shows up when $k_\parallel$ becomes finite, as demonstrated in Fig. 4 for $k_\parallel = 0.14\ \mathrm{nm}^{-1}$, where panel (a) is for $|\psi_+(y)|^2$ and panel (b) is for $|\psi_-(y)|^2$. While the $1e$ state and the $1lh$ state are strongly coupled, the $1e$ state also couples to the $2hh$ state. This is the reason why both the $1e$ wave function and the $1lh$ wave function have significant amplitude in the GaSb layer, where the $1e$, $1lh$, and $2hh$ wave functions are heavily distorted.

With increasing the layer thickness of InAs and/or GaSb, the spatial confinement gets weaker and so more subbands appear in the quantum well. Here we discover an interesting phenomenon that a heavy-hole subband lies in the wide hybridization gap between an electron subband and a light-hole subband. The subband structure for the broken-gap quantum well with an 18 nm thick InAs layer and a 12 nm thick GaSb layer is shown in Fig. 5, with panel (a) for "spin-up" states and panel (b) for "spin-down" states. The physics around the zone center is not affected qualitatively because at zone center only the heavy-hole states are still decoupled from all other states. Also, the characteristic behavior of the $1lh$-$1hh$-$2hh$ multiple anticrossing is not sensitive to the width of the quantum well. However, a qualitatively new feature appears around $k_\parallel = 0.2\ \mathrm{nm}^{-1}$, where the strong hybridization between the $1e$ and the $1lh$ subbands creates a large gap. In panel (a) the $3hh$ subband passes through this gap almost unperturbed. On the other hand, in panel (b) the $3hh$ subband is pushed upward by the $1e$ subband due to the energy closeness of the subbands. This difference indicates a possible spin-dependent coupling between electron states and heavy-hole states.

To clarify this aspect, we show the probability density $|\psi_+(y)|^2$ in Fig. 6, and $|\psi_-(y)|^2$ in Fig. 7. In both figures, the values of $k_\parallel$ are $0.18\ \mathrm{nm}^{-1}$ for panel (a) and $0.2\ \mathrm{nm}^{-1}$ for panel (c). For panel (b), we have $k_\parallel = 0.19\ \mathrm{nm}^{-1}$ for Fig.

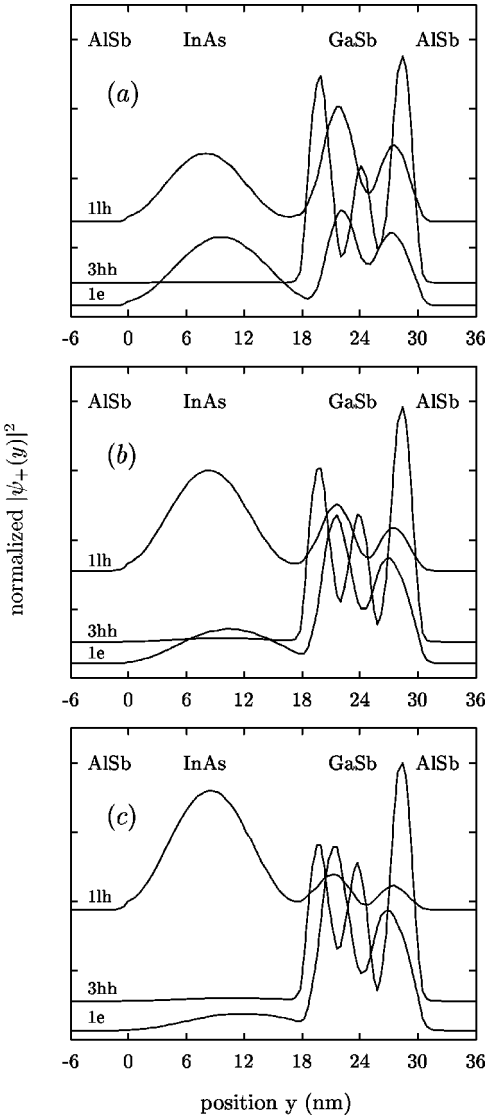

FIG. 6. Normalized probability density $|\psi_+(y)|^2$ of the $1e$, $3hh$, and $1lh$ "spin-up" states at $k_\parallel = 0.18$ nm^{-1} [panel (a)], $k_\parallel = 0.19$ nm^{-1} [panel (b)], and $k_\parallel = 0.2$ nm^{-1} [panel (c)] in a quantum well with an 18 nm InAs layer and a 12 nm GaSb layer.

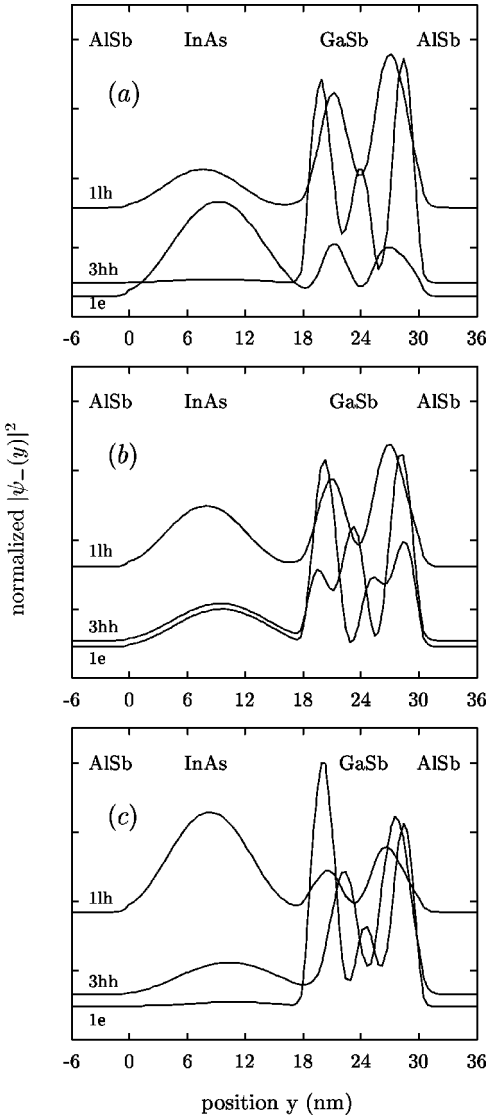

FIG. 7. Normalized probability density $|\psi_-(y)|^2$ of the $1e$, $3hh$, and $1lh$ "spin-down" states at $k_\parallel = 0.18$ nm^{-1} [panel (a)], $k_\parallel = 0.188$ nm^{-1} [panel (b)], and $k_\parallel = 0.2$ nm^{-1} [panel (c)] in a quantum well with an 18 nm InAs layer and a 12 nm GaSb layer.

6, but $k_\parallel = 0.188$ nm^{-1} for Fig. 7. A strong hybridization between the electron states and the light-hole states is seen in all cases, leading to a profound anticrossing of the $1e$ subband and the $1lh$ subband. However, a strong mixing of the heavy-hole states and the electron states appears only in Fig. 7 for the "spin-down" states. We see in Fig. 7 that the $3hh$ state no longer remains unperturbed from the electron states. Instead, the wave function of the $3hh$ state spreads over the whole coupled quantum wells at $k_\parallel = 0.188$ nm^{-1}, indicating a strong mixing with the electron states. Furthermore, since there is also a strong mixing between the $1e$ and the $1lh$ states, we conclude that the electron, the heavy-hole, and the light-hole states couple strongly with one another. As a consequence of this mixing, as $k_\parallel$ approaching 0.2 nm^{-1}, the $1e$ state becomes heavy-hole-like, the $1lh$ state becomes electronlike, and the $3hh$ state becomes light-hole-like state. With further increase of $k_\parallel$, the $1e$ state turns into light-hole-like, and the $3hh$ state goes back to heavy-hole-like.

V. CONCLUSION

We have investigated the in-plane dispersions of AlSb/InAs/GaSb/AlSb broken-gap quantum wells, using the eight-band $\mathbf{k}\cdot\mathbf{p}$ model and the scattering matrix algorithm. The wide hybridization gaps resulting from the strong mixing between the electron states and the light-hole states are found to be spin dependent. The magnitude and the position of the hybridization gaps in the dispersion relations are sensitive to the widths of the InAs layer and the GaSb layer. Quantum wells with thick layers exhibit multiple anticrossing for which the heavy-hole subband lies in the hybridization gap

produced by the mixing of the electron subband and the light-hole subband. Depending on the spin state, at the anticrossing point the heavy-hole subband may remain almost unperturbed, or the heavy-hole may spread over the entire quantum well.

ACKNOWLEDGMENTS

The financial support of the National Science Council of ROC to A.Z. and to S.T.Y. (Grant No. NSC90-2112-M-259-004) is acknowledged.

[1] D.Z.-Y. Ting, D.A. Collins, E.T. Yu, D.H. Chow, and T.C. McGill, Appl. Phys. Lett. **57**, 1257 (1990).
[2] J.F. Chen, and A.Y. Cho, J. Appl. Phys. **71**, 4432 (1992).
[3] Y.H. Wang, M.H. Liu, M.P. Houng, J.F. Chen, and A.Y. Cho, IEEE Trans. Electron Devices **41**, 1734 (1994).
[4] M.H. Liu, Y.H. Wang, M.P. Houng, J.F. Chen, and A.Y. Choe, Jpn. J. Appl. Phys. **35**, 1178 (1996).
[5] J. Katz, Y. Zhang, and W.I. Wang, Appl. Phys. Lett. **62**, 609 (1993).
[6] C. Jenner, E. Corbin, B.M. Adderley, and M. Jaros, Semicond. Sci. Technol. **13**, 359 (1998).
[7] A.N. Baranov, N. Bertru, Y. Cuminal, G. Boissier, C. Alibert, and A. Joullie, Appl. Phys. Lett. **71**, 735 (1997).
[8] M.J. Yang, F.C. Wang, C.H. Yang, B.R. Yang, B.R. Bennett, and T.Q. Do, Appl. Phys. Lett. **69**, 85 (1996).
[9] M. Dmdic, M.P. Grimshow, L.J. Cooper, D.A. Ritchie, and N.K. Patel, Appl. Phys. Lett. **70**, 481 (1997).
[10] M.J. Yang, C.H. Yang, B.R. Bennett, and B.V. Shanabrook, Phys. Rev. Lett. **78**, 4613 (1997).
[11] L.J. Cooper, N.K. Patel, V. Drouot, E.H. Linfield, D.A. Ritchie, and M. Pepper, Phys. Rev. B **57**, 11 915 (1998).
[12] M. Lakrimi, S. Khym, R.J. Nicholas, D.M. Symons, F.M. Peeters, N.J. Mason, and P.J. Walker, Phys. Rev. Lett. **79**, 3034 (1997).
[13] A.J.L. Poulter, M. Lakrimi, R.J. Nicholas, N.J. Mason, and P.J. Walker, Phys. Rev. B **60**, 1884 (1999).
[14] M. Altarelli, Phys. Rev. B **28**, 842 (1983).
[15] A. Fasolino and M. Altarelli, Surf. Sci. **142**, 322 (1984).
[16] M. Altarelli, J.C. Maan, L.L. Chang, and L. Esaki, Phys. Rev. B **35**, 9867 (1987).
[17] J.C. Chiang, S.F. Tsay, Z.M. Chau, and I. Lo, Phys. Rev. Lett. **77**, 2053 (1996).
[18] Y.X. Liu, R.R. Marquardt, D.Z.-Y. Ting, and T.C. McGill, Phys. Rev. B **55**, 7073 (1997).
[19] S. de-Leon, L.D. Shvartsman, and B. Laikhtman, Phys. Rev. B **60**, 1861 (1999).
[20] M.S. Kiledjian, J.N. Schulman, K.L. Wang, and K.V. Rousseau, Phys. Rev. B **46**, 16 012 (1992).
[21] D.Z.-Y. Ting, E.T. Yu, and T.C. McGill, Phys. Rev. B **45**, 3583 (1992).
[22] L.-W. Wang, S.H. Wei, T. Mattila, A. Zunger, I. Vurgaftman, and J.R. Meyer, Phys. Rev. B **60**, 5590 (1999).
[23] R. Magri, L.W. Wang, A. Zunger, I. Vurgaftman, and J.R. Meyer, Phys. Rev. B **61**, 10 235 (2000).
[24] Y. Noveh and B. Laikhtman, Appl. Phys. Lett. **66**, 1980 (1995).
[25] E. Halvorsen, Y. Galperin, and K.A. Chao, Phys. Rev. B **61**, 16 743 (2000).
[26] M.G. Burt, J. Phys.: Condens. Matter **4**, 6651 (1992).
[27] B.A. Foreman, Phys. Rev. B **56**, R12 748 (1997).
[28] D.Y.K. Ko and J.C. Inkson, Phys. Rev. B **38**, 9945 (1988).